SJSR Singapore Journal of Scientific Research

OPEN ACCESS

Corrosion Inhibition and Antimicrobial Studies of Imine Chelator and its M(II) Chelates: Synthesis and Characterizations

[1]Theresa Chizoba Wodi, [2]Chioma Donubari Don-Lawson and [1]Chioma Festus

[1]Department of Chemistry, Ignatius Ajuru University of Education, Rumuolumeni, Port Harcourt, Rivers State, Nigeria

[2]Department of Chemistry, Rivers State University, Port Harcourt, River State, Nigeria

ABSTRACT

Background and Objective: Organic molecules with non-carbon atoms, have found applications in many fields of life science and technology. They constitute the vast majority of the molecules involved in the operations of man in exerting control over nature. Thus, studies of some bivalent metal chelates of bidentate imine-chelator (LH) acquired from 2-hydroxyl-1-naphthaldehyde (2-HNA) and 2-amino-6-ethoxybenzothiazole (2-AEBT). **Materials and Methods:** The synthesis, characterization and corrosion inhibition studies were carried out via facile reactions, analytical spectral, theoretical and inhibitive methods reported in our previous works. The antimicrobial properties of the synthesized compounds were tested *in vitro* against *P. mirabilis*, *E. coli*, *S. aureus*, *K. oxytoca*, *S. Epidermidis*, *S. Pneumoniea*, *A. niger*, *A. flavus and Fuserium* sp., strains. **Results:** The vibrational spectra of LH revealed a band at 1622 cm^{-1}, which was ascribed to the -C=N- stretching vibration which appeared at lower frequencies in the chelates' spectra indicating chelation. Jobs' method of continuous variation suggests 1:2 metal to ligand ratio. The effect of LH and its chelates on acid deterioration of mild steel (ms) was visible indicating that LH had considerable corrosion inhibition (CI) performance in contrast to corrosion of ms in a 1M HCl solution. The premeditated zinc complex had the best antibacterial activity while the manganese complex showed enormously fine antifungal actions against the screened microbes with inhibitory zones of 15.0 and 26.5 mm separately. **Conclusion:** The synthesized compounds had the highest antibacterial and antifungal actions against *Streptococcus* sp., *A. niger*. The absorption of the compounds on the metal surface was proven by the Density Functional Theory (DFT) calculations showing they are potential corrosion inhibitors for steel protection.

KEYWORDS

Corrosion-inhibition, imine chelator, hydroxynaphthaldehyde, ethoxybenzothiazole, DFT studies

INTRODUCTION

Schiff-based compounds are important and widely used for various functions due to their high thermal and moisture stability at different temperatures[1,2]. They are used as optical materials, polymers, dyes, pigments, steel/iron corrosion inhibitors, as well as for heavy metal spectral analysis and as catalysts in various related reactions to high temperatures[3,4]. Schiff bases (SBs) have been used to produce novel

ISSN: 2152-0461 (Online)
ISSN: 1816-4919 (Print)
https://doi.org/10.17311/sjsr.2023.10.25

Received: 15 Dec. 2022
Accepted: 13 May, 2023
Published: 24 May, 2023

chemotherapeutic compounds[5] because many of them serve as models for biological species in the field of bio-inorganic[6]. Many SB compounds exhibit remarkable catalytic activities owing to the presence of H_2O vapor[7]. Recently, there has been renewed interest in SB complexes due to the search for drugs with better overall therapeutic effects while being less hazardous[8]. Due to the complexity involved in biological systems, the reactivity of these compounds has increased biologically and their inherent chemical benefits as polydentate chelators have promoted the increase in discovering their coordinated behavior[9].

The thiazole ring is important due to its content. Penicillin, the first and foremost broad-spectrum antibiotic contains tetrahydrothiazole in its structure[10]. Thiazole and thiazolamine are essential drugs[11]. Several biological activities are known to be conceivable for compounds with thiazole and 2-aminothiazole rings[12,13]. In pharmacology, 2-aminothiazole derivatives are widely used. They also have antibacterial and antioxidant properties. Several aminothiazole substitutes are used as antioxidant additives in hydrocarbons, minerals and synthetic lubricants, as well as solid paraffins, polyolefins and vegetable fats[14]. Triazine derivatives with 2-aminothiazole moiety are active anti-scratch, anti-wear and anti-corrosion additives for lubricating oils. Rust, especially in humid atmospheres and acidic environments, is a major obstacle to the widespread use of MS in most industries, as it is widely used for structural purposes[15]. In general, industries use acids for pickling and cleaning structural steel and these processes are always complicated by significant metal decomposition[15]. However, the use of inhibitors remains the most effective corrosion prevention technique[16].

Organic compounds with heteroatoms in aromatic rings are often used as corrosion inhibitors. These compounds have the ability to adsorb onto metal surfaces and block active sites on the surface, thereby reducing the rate of corrosion. Many chelator-inhibitors have demonstrated good corrosion inhibitory properties at different temperatures in different acidic environments[17]. The most effective corrosion inhibitors such as organic molecules with polar functional groups such as sulfur, oxygen and nitrogen have conjugated systems and hydrophobic components that help to protect metals from corrosive environments[18]. Previously, our research group synthesized and investigated the CI potential of several 2-(thiazol-2-ylamino)-2,3-dihydonaphthalene-1-4-dione complexes[19]. This study presented the synthesis of SB formed by condensing 2-hydroxyl-1-naphthaldehyde with 2-amino-6-ethoxybenzothiazole, its complexation with transition elements and its antimicrobial and anti-corrosion activities.

MATERIALS AND METHODS

Study area: This work was carried out within 3 months (March to June, 2021) in the research laboratory of the Department of Chemistry at Ignatius Ajuru University of Education, Rivers State, Nigeria.

Materials: Divalent acetate salts (Mn, Ni, Cu and Zn), sulfate (Fe) and chloride (Co), Zn-dust, 2-hydroxyl-1-naphthaldehyde (2-HNA), 2-amino-6-ethoxybenzothiazole (2-AEBT), purchased from Aldrich Coy Germany. To document the infrared and electronic spectra of the compounds, the Perkin Elmer Spectrum-100 spectrometer with KBr plates and the PEKIN ELMER LAMBDA 25UV/VISIBLE spectrometer (190-900 nm) were used independently. The magnetic sensitivity of the synthesized chelates was investigated using Festus and Don-Lawson's Method[20]. The antibacterial and antifungal experiments were performed exactly as Festus *et al.*[21].

Synthesis of the chelator and divalent chelates: The chelator (Scheme 1) was prepared by dissolving 11.26 and 10.00 g of 2-AEBT and 2-HNA in a 30 mL ethanol solution. The resulting solution was refluxed for 6 hrs. with stirring. The resulting pale yellow precipitate was filtered and recrystallized with C_2H_5OH[22]. The imine-chelator bivalent metal chelates were synthesized by reacting the calculated sum of the chelator (LH, 1.1 g, 1.58×10-3 mL) and the respective metal (0.387, 0.44, 0.375, 0.39, 0.32 and 0.35 g of Mn(II), Fe(II), Co(II), Ni(II), Cu(II) and Zn(II)) salts in 2:1 ratio according to a method published in the literature[23] (Scheme 1 and 2). The resulting compounds were dried on anhydrous $CaCl_2$ and analytical data[24] were presented in Table 1.

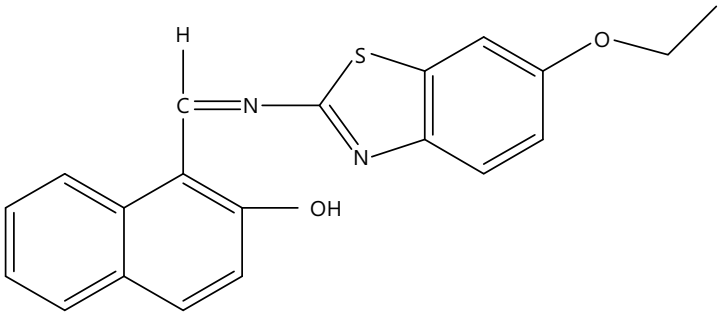

Scheme 1: Proposed structure of the Schiff base ligand

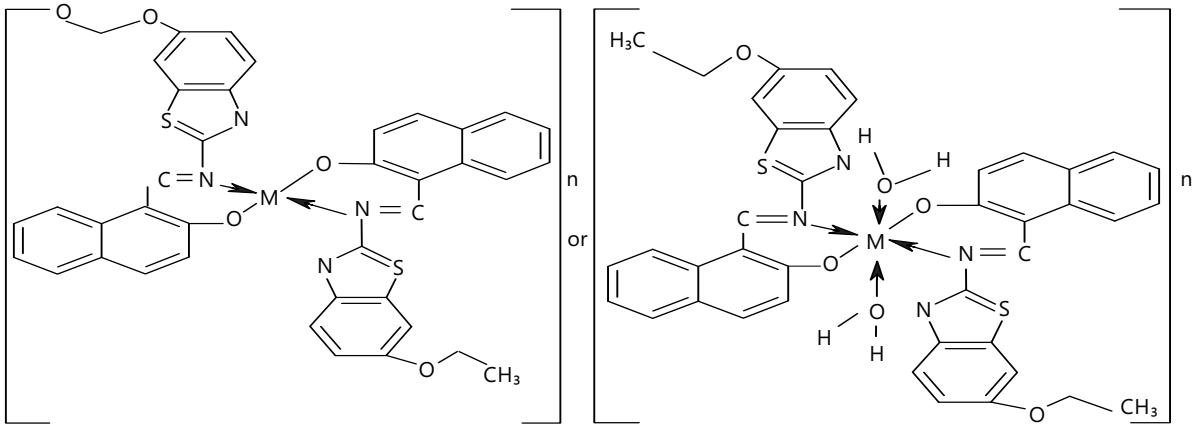

Scheme 2: Proposed structure of the metal(II) complexes

Corrosion inhibition studies

Preparation of MS coupons: The MS sheet obtained from Rivers State University with approximate compositions: C (0.120%), Mn (9.0×10^{-1} %), S (6.6×10^{-2} %), P (5×10^{-2} %), Si (1×10^{-1} %) and Fe (98.314%), of thickness 0.5 and 0.7 mm was cut into rectangular coupons of dimensions 40/40 and 50/40 mm. The coupons were prepared following a literature method[25,26].

Gravimetric measurements: A mole of HCl solution was prepared by diluting 37% HCl reagent grade with twofold distilled H_2O. For inhibition investigations, different amounts of inhibitor solutions were produced by dissolving the required amount of LH and its bivalent chelates in 50 mL of 1M HCl. A blank test solution of 100 mL of 1M HCl without the inhibitor was prepared. The weight loss experiment was carried out exactly as described by Festus and Wodi[18].

Characterization techniques

FT-IR SPECTRA: The FTIR of the chelator plus its M(II) complexes were accounted on a PERKIN ELMER FI-IR SPECTRUM BX Spectrophotometer using KBr disc in the scale 4000-350 cm^{-1} at the Department of Chemistry, University of Ibadan, Nigeria. The relevant band positions and their apportioning were presented in Table 2.

Electronic spectra data: The UV-vis spectra measurement of the chelator plus its M(II) complexes were recorded on PEKIN ELMER LAMBDA 25UV/VIS spectrophotometer within the scale 190-400 and 400-900 nm at the Department of Chemistry, University of Ibadan, Nigeria. The UV-visible spectral data of the synthesized compounds were shown in Table 3.

Table 1: Physicochemical data of the imine chelator and its M(II) chelates

Compound	Molecular weight	M. Pt(°C)/yield (%)	Shade	μ*eff* (BM)	Ohm^{-1} cm^2 mol^{-1}
LH $C_{2o}H_{15}O_2N_2S$	347.01	180-183/76	Yellow	-	-
$[Mn(L)_2(H_2O)_2]$ $MnC_{40}H_{34}O_6N_4S_2$	975.702	210-212/51	Deep brown	6.81	09.3
$[Fe(L)_2(H_2O)_2]$ $FeC_{40}H_{34}O_6N_4S_2$	928.834	194-197/70	Brown	6.77	28.7
$[Co(L)_2]H_2O$ $CoC_{40}H_{32}O_5N_4S_2$	968.542	245-247/41	Dark brown	4.93	37.2
$[Ni(L)_2(H_2O)]$ $NiC_{40}H_{32}O_5N_4S_2$	979.462	239-242/33	Oxy-blood brown	4.0	20.1
$[Cu(L)_2(H_2O)_2]$ $CuC_{40}H_{34}O_6N_4S_{22}$	937.104	230-232/69	Light brown	2.2	33.9
$[Zn(L)_2(H_2O)_2]$ $ZnC_{40}H_{34}O_6N_4S_2$	986.124	280-283/70	Orange	0.76	15.9

Table 2: FTIR of the Imine chelator, LH and its bivalent metal chelates

Compound	LH	$[Mn(L)_2(H_2O)_2]$	$[Fe(L)_2(H_2O)_2]$	$[Co(L)_2(H_2O)_2]$	$[Ni(L)_2(H_2O)]$	$[Cu(L)_2(H_2O)_2]$	$[Zn(L)_2(H_2O)_2]$
OH/H_2O	3337	3417	3433	3418	3420	3422	3425
-C=N	1622	1621	1622	1617	1620	1616	1618
-C=C	1601	1601	1602	1601	1602	1660	1601
Aromatic C-N	1232	1270	1232	1230	1213	1264	1231
Stretch C-O	1057	1142	1059	1058	1062	1066	1058
C-H Stretch	2926	2977	2978	2976	2925	2977	2976
Aliphatic C-C	1036	1058	1036	1041	1062	1042	1042
C-S	813	813	813	829	834	826	832
C-C Stretch (n ring)	1574	1574	1575	1576	1578	1573	1581
=C-H Aromatic	-	-	-	3059	-	3059	3041
CH rocking in plane	748	743	743	744	750	745	744
OH bending	942	942	964	975	979	984	974
=C-H aromatic bend	-	-	942	941	943	946	942
CH_2 in plane bending	1450	1450	1457	1453	1439	1453	1455
CH_3 bend	-	-	-	1376	1365	1378	1379
M-N	-	591	616	633	686	633	590
M-O	-	487	433	492	658	499	493

Table 3: Electronic absorption (cm^{-1}) spectra data of the compound

Compounds	Absorption	Band assignment	Geometry
LH	40323	CT	Octahedral
	33784		
	19531		
$[Mn(L)_2(H_2O)_2]$	39841, 33898	π→π*	
	25000	n→π*	
	16611	$^6A_{1g}\rightarrow{}^4T_{1g}$	
	15674	$^6A_{1g}\rightarrow{}^4T_{1g}$	
	14641	$^6A_{1g}\rightarrow{}^4T_{2g}$	
$[Fe(L)_2(H_2O)_2]$	40161	CTT	Octahedral
	33784, 33003	π→π*	
	29,851	n→π*	
	16,077	$^5T_{2g}\rightarrow{}^5E_{1g}$	
	14,684	$^4T_{2g}\rightarrow{}^5E_{1g}$	
$[Co(L)_2(H_2O)]$	39,841	π→π*	Octahedral
	15,625	$^4T_{1g}\rightarrow{}^4A_{2g}$	
	14771	$^4T_{1g}\rightarrow{}^4A_{2g}$	
$[Ni(L)_2](H_2O)$	39841, 33784	π→π*	Tetrahedral
	15649	$^3T_1\rightarrow{}^3T_1(F)$	
	14706	$^2A_1\rightarrow{}^3T_1(F)$	
$[Cu(L)_2(H_2O)_2]$	39683, 33784	π→π*	Octahedral
	15924	$^2E_g\rightarrow{}^2T_{2g}$	
	14728, 13123	$^2B_{1g}\rightarrow{}^2A_{1g}$	
$[Zn(L)_2(H_2O)_2]$	40323	M-LCT	Octahedral
	18416, 15456		

Molar conductance measurement: An electronic conducting set HANNA HI 991 300 conductivity meter of 1.0 cell constant was used to carry out the molar conductivity measurements in $(CH_3)_2SO$. A 1×10^{-3} mold m^{-3} solution of the M(II) complexes were prepared and allowed to reach room temperature before measuring their respective conductivities as seen in Table 1.

Magnetic susceptibility measurement: The magnetic susceptibilities of the synthesized complexes were examined at the Inorganic Chemistry Laboratory Department of Chemistry, University of Ibadan, on a Johnson Mathey magnetic balance at a room temperature range of 27-32°C while magnetically dilute corrections were calculated using Pascal's constant. The μ*eff* results were presented in Table 1.

Biological studies

Antibacterial activities: Antibacterial activities of LH and its bivalent chelates were assessed on six microbial strains *S. aureus*, *E. coil*, *S. Epidermis*, *K. oxytoca*, *S. pneunoniea* and *P. mirabilis* via a disc diffusion method[18,20]. Streptomycin was utilized as a positive control.

Antifungal activity: The chelator and its M(II) chelates were further tested for anti-fungal activity against three fungal strains: *A. flavus*, *Fuserium* sp. and *A. niger*. The positive control was miconaozole, while the obtained results were analyzed according to Festus *et al.*[21].

RESULTS AND DISCUSSION

Physiochemical data: The synthesized compounds were typically colored solids that were soluble in organic solvents but varied in their stability in the air. Acquired data denotes a molar ratio of 1:2 of M-L, which supported the stoichiometry of the type $[M(L)_2]$ and $[M(L)_2(H_2O)_2]$ for the 4- and 6-coordinate chelates, respectively. The molar conductance values found in $(CH_3)_2SO$ were very low (9.3-37.2 ohm^{-1} cm^2) to allow complex dissociation and indicated the complexes' non-electrolytic character. Except for Zn(II) chelate, which was diamagnetic, the μ*eff* result indicated that other chelates were paramagnetic (Table 1). The μ*eff* values of the chelates at room temperature were also compatible with a 6-coordinate assemblage, with the exception of Ni(II) chelate, which revealed tetrahedral geometry. The chelates had greater melting points than the parent imine chelator, indicating that they were more stable than the imine chelator.

FT-IR spectra: The stretching vibrations of the imine chelator, LH and its chelates. With an absorption band at 1622 cm^{-1}, the infrared spectra of LH indicated the formation of imine bonds (-C=N-) and the lack of carbony1 bonds (C=O) as shown in Table 2. The latter was present in the chelates as well, albeit at lower wavenumbers between 1616 and 1620 cm^{-1}, indicating the participation of the imine N-atom in coordinating with the M(II) ions[27]. Similarly, at 1600-1602 cm^{-1}, the stretching vibration of C=C groups was seen in the spectra of LH and its chelates. A broad absorption band at 3337 cm^{-1} was ascribed to intra-molecular H-bonding vibration (O-H), which was frequently observed in imine chelators containing hydroxyl groups[28,29]. The detected OH bending vibration at 942 cm^{-1} in the chelator shifted to a higher wavenumber in the chelates, demonstrating the existence of H_2O molecules[30,31]. The weak absorption bands found in the chelates of $[Co(L)_2(H_2O)_2]$, $[Cu(L)_2(H_2O)_2]$ and $[Zn(L)_2(H_2O)_2]$ were assigned to the (=C-H) aromatic stretching vibration, whereas, the (C-H) aliphatic asymmetric stretching band was detected at 2926 cm^{-1} but moved to a higher wavenumber (2976-2978) cm^{-1} in the spectra of the chelates. Furthermore, C-O absorptions between 1057-1142 cm^{-1} suggest the existence of an alcohol/phenol group[32]. A sharp but short intensity band at 1213-1264 cm^{-1} was designated for stretching vibration of N(C-N) automatic group[33]. This band shifted to emerge as a sharp albeit medium intensity band in the chelates' spectra between 813-834 cm^{-1} [34]. The LH acted as an asymmetric bi-dentate chelator composed of N and O atoms from amine and carbonyl moieties. Due to the participation of carbonyl O and deprotonated amine N atoms binding to the M(II) ions, two additional bands at 633-588 and 403-499 cm^{-1} formed in the far infrared portion of the complexes' spectra, indicating the establishment of metal to nitrogen (M-N) and metal to oxygen (M-O) bonds[35].

Electronic spectral, molar conductivity and magnetic moment measurements: The compounds' UV-vis spectra revealed intra-chelator (n→π*, π→π*) and intra/inter chelates (d-d, L→MCT) transitions. The geometries of the chelates were assigned based on electronic absorptions and μ*eff* data[30,36]. The ultraviolet spectra of the imine chelator as seen from Table 3, showed three bands. The bands at 40323 and 33784 cm^{-1} were caused by charge transfer and π→π* transitions in the LH naphthalene unit[30,37]. The latter also appeared at lesser wavenumbers within the spectra of the bivalent chelates due to chelation of the LH with the M(II) ions. The bands assigned to intra-LH (π→π*) for $[Mn(L)_2(H_2O)_2]$, $[Fe(L)_2(H_2O)_2]$, $[Co(L)_2(H_2O)_2]$, $[Ni(L)_2](H_2O)$ and $[Cu(L)_2(H_2O)_2]$ chelates were observed at 39841 and 33898, 33784 and 33003, 39841, 39841 and 33784 and 39683 and 33784 cm^{-1} correspondingly as presented from Table 3. Based on LH field transitions, the spectra of $[Fe(L)_2(H_2O)_2]$ and $[Zn(L)_2(H_2O)_2]$ chelates revealed additional low intensity bands in the visible area[38]. The $[Mn(L)_2(H_2O)_2]$ chelate exhibited a band at 25000 cm^{-1} that might be attributed to a n→π* transition associated with imine moiety coupling[24]. Other bands at 16611, 15674 and 14641 cm^{-1} were ascribed to $^6A_{1g}\rightarrow{}^4T_{1g}(G)$, $^6A_{1g}\rightarrow{}^4T_{1g}$ and $^6A_{1g}\rightarrow{}^4T_{2g}(G)$ transitions respectively typical of a 6-coordinate assemblage. The Fe(II) chelates are found in coordination sites that are near octahedral and tetrahedral symmetry[39]. The $[Fe(L)_2(H_2O)_2]$ chelate demonstrated an n→π* transition at 29851 cm^{-1}, with large bands owing to Jahn Teller effects at 16077 and 14684 cm^{-1} attributable to the $^5T_2g\rightarrow{}^5Eg$ transition and compatible with a 6-coordinate geometry[31]. High spin Co(II) chelates with $^4T_2(t_{25}e^2)$ and $^2E(t_{26}e^1)$ configurations frequently exhibit spin crossover equilibrium[30]. Two absorption bands at 15625 and 14771 cm^{-1} in the visible spectra of the $[Co(L)_2(H_2O)_2$ chelate were identified and ascribed to $^4T_{1g}\rightarrow{}^4A_{2g}$ and $^4T_{1g}\rightarrow{}^4T_{1g}(P)$ transitions corresponding to a d^7 high spin octahedral system with 4^F ground term[40]. The assignment of high spin 6-coordinate assemblage to the latter was verified by the calculated μ*eff* of 4.9BM since μ*eff* of Co(II) chelates were likely to be higher than the spin-only value for 6-coordinate octahedral chelates due to orbital contributions[27,36]. Two visible spectral bands at 15549-14706 cm^{-1} were ascribed to the $^3A_{2g}\rightarrow{}^3T_{1g}(F)$ transition by the Ni(II) chelate. An μ*eff* of 4.0 BM found for the Ni(II) chelate supported the attribution to tetrahedral assembly. Bivalent nickel chelates with a tetrahedral structure are paramagnetic, with μ*eff* values ranging from 3.70 to 4.0 BM[41]. The spectra of Cu(II) chelate showed a wide band at 13123, 14728 and 15924 cm^{-1} ascribed to the $^2E_g\rightarrow{}^2T_{2g}$ transition induced by Jahn-Teller distortion 6-coordinate assemblage[39]. The absence of bands below 10,000 cm^{-1} ruled out a tetrahedral shape. The visible spectra of the Zn(II) chelate did not display any d-d transition band, which is typical with Zn(II) chelates. The chelates' molar conductivity values (Table 1) were in the range of 9.3-37.2^{-1} cm^{-2} mol^{-1}, indicating their non-electrolytic character.

Biological studies

Antibacterial activities: Antibacterial activities of LH and its bivalent chelates were assessed on six microbial strains *S. aureus*, *E. coil*, *S. Epidermis*, *K. oxytoca*, *S. pneunoniea* and *P. mirabilis* via a disc diffusion method[42]. Streptomycin was utilized as a positive control. The antibacterial results (Table 4) demonstrated that, with the exception of *P. mirabilis*, the tested chelates were active against the microorganisms. This

Table 4: Anti-bacteriological actions of LH and its bivalent metal chelates

	Bacterial organisms						Fungal organisms		
Compound	*S. aureus*	*E. coli*	*S. epidermidis*	*K. oxytoca*	*S. pneumoniea*	*P. mirabilis*	*A. flavus*	*Fuserium* sp.	*A. niger*
LH	0.0±0.0	0.0±0.0	0.0±0.0	8.0±0.0	0.0±0.0	0.0±0.0	15.5±0.5	6.0±0.0	23.0±1.0
$[Mn(L)_2(H_2O)_2]$	0.0±0.0	0.0±0.0	8.0±0.0	0.0±0.0	0.0±0.0	0.0±0.0	17.5±0.5	8.0±0.0	26.5±0.5
$[Fe(L)_2(H_2O)_2]$	6.5±0.0	4.0±0.0	0.0±0.0	6.5±0.0	6.0±0.0	0.0±0.0	21.0±1.0	21.0±1.0	20.5±0.5
$[Co(L)_2(H_2O)_2]$,	5.5±5.0	0.0±0.0	8.0±0.0	0.0±0.0	0.0±0.0	0.0±0.0	13.0±1.0	0.0±0.0	26.0±0.0
$[Ni(L)_2]H_2O$	0.0±0.0	0.0±0.0	9.0±1.0	0.0±0.0	0.0±0.0	0.0±0.0	11.5±0.5	0.0±0.0	25.0±1.0
$[Cu(L)_2(H_2O)_2]$	0.0±0.0	0.0±0.0	0.0±0.0	0.0±0.0	4.5±0.5	0.0±0.0	12.0±0.0	14.5±0.5	26.0±0.0
$[Zn(L)_2(H_2O)_2]$	11.0±1.0	0.0±0.0	0.0±0.0	0.0±0.0	15.0±1.0	0.0±0.0	14.0±0.0	20.0±0.0	22.0±0.0
Streptomycin/ miconazole	14.0±0.0	15.0±1.0	11.0±1.0	12.0±0.0	13.5±0.5	9.0±1.0	8.0±0.0	0.0±0.0	10.0±0.0

might be related to the chelation effect, which boosts antibacterial activities principally due to the partial dispersion of oxidative charge resident on the M^{2+} with LH heteroatoms and possible electron delocalization on the cyclic rings[38,43]. $Zn(L)_2(H_2O_2)$ chelates inhibited *S. pneumoniea* more effectively, with inhibitory zones of 9.0 and 15.0 mm, respectively. The chelator was exclusively effective against *K. oxytoca*. The Ni(II) plus Zn(II) chelates repressed *S. pneumoniea* more efficiently, with inhibitory zones of 9.0 and 15.0 mm, respectively. The sensitivity of Ni(II) and Zn(II) chelates could be attributed to bacterial organisms producing potent protein toxins to activate their cell surface proteins, preventing adequate permeation of the chelates into the bacteria cells, as well as lower lipophilicity of the chelates, which also reduces their penetration through the lipid cell membrane[30]. The Mn(II) plus Ni(II) chelates remained inactive against all the microbes except *S. epidermidis*. $[Fe(L)_2(H_2O)_2]$ remained active against 4 organisms, *S. aureus*, *E. coil*, *K. oxytoca* and *S. pneumoniea* with inhibitory zones range of 4.0-7.0 mm. $[Co(L)_2H_2O_2]$ had a little antibacterial effect on *S. aureus* and *S. epidermidis* but did not affect other bacterial species. Except for *S. pneumoniea*, which showed an inhibitory zone of 5.0 mm, the $[Cu(L)_2(H_2O]$ chelate had no effect against all bacteria species. The inhibitory zone of $Zn(L)_2(H_2O)_2$ against *S. pneumoniea* was 15.0 mm, which was more than the antibacterial medication employed. The superior antibacterial activity of the $Zn(L)_2(H_2O)_2$ complex over the comparable chelating drugs may be explained using the overtone idea and Tweedy's chelation theory[30].

According to the overtone notion of cell permeability, the hydrophobicity of the lipid membrane that surrounds the cell enables only lipid-soluble molecules to pass through, which is a vital factor that affects anti-microbial action[44,45]. The polarity of the metal ion is greatly reduced during chelation due to chelator orbital overlap and partial sharing of the metal ion's positive charge with donor groups. Furthermore, it promotes the delocalization of elections across the whole chelate ring and increases the lipophilicity of the chelates[1]. This enhanced lipophilicity facilitates the entry of chelates into lipid membranes, halting the numerous metabolic processes of microorganisms. The enhanced activity of chelates can be attributed to the presence of an M^+ ion in normal cell activities[46].

Antifungal activity: The chelator and its M(II) chelates were further tested for anti-fungal activity against three fungal strains: *A. flavus*, *Fuserium* sp. and *A. niger*. The positive control was miconaozole. The antifungal results (Table 4) revealed that $[Mn(L)_2(H_2O)_2]$ had the most potent antifungal activity against *A. niger*. Antifungal activities revealed that the chelator had a lower inhibitory impact on the fungus with inhibition zones lower than its chelates. However, after coordination with metal ions, the latter's effects were more effective and prominent. This increase might be attributed to chelate toxicity, which is caused by a synergistic impact between the metal ion and the Lewis base. Other aspects that may have contributed to the chelates' improved antifungal activity include chelation and a greater steadiness constant. All The chelates displayed comparable inhibitory zones with *A. flavus* and *A. niger* to the conventional medication[38,47]. When compared to the usual medication, the bivalent chelates demonstrated more pronounced antifungal activity.

CI-Data

Gravimetric measurements: Gravimetric measurements of ms were performed at 303K in the absence and presence of 100-500 ppm uniform complex solution to investigate the influence of LH and its chelates on corrosion of ms in 1M HCl. As a control, a 100 ppm blank solution with no chemical was used. Table 5 and Fig. 1a-b show the percentage (%) IE and CR determined from weight decreases over 5 hrs. The research showed that LH and its chelates have significant CI potentials in comparison to ms corrosion in a 1M HCl solution. The better inhibitory result of LH might be attributed to chelation via the donor-acceptor interaction between the undistributed electron pairs of LH donor atoms and metal ions[48,49]. The chelates outperformed the uncoordinated LH in terms of IE. The latter may be attributable to the chelates' huge masses and molecular planarity. Table 6 summarized the findings of CR, Θ and IE

Table 5: Weight, IE (%) and CR obtained for a MS immersed in 1M HCl of the compounds at 303K for 5 hrs

Compound	Concentration	CR	IE (%)	Θ	W
LH	Blank	0.0053	-	-	0.0265
	100	0.0042	20.75	0.2075	0.0210
	200	0.0038	28.30	0.2830	0.0190
	300	0.0007	86.79	0.8679	0.0035
	400	0.0004	92.45	0.9245	0.0020
	500	0.0003	94.34	0.9434	0.0015
$[Mn(L)_2(H_2O)_2]$	Blank	0.0042	-	-	0.0210
	100	0.0006	85.71	0.8571	0.0030
	200	0.0004	90.48	0.9048	0.0020
	300	0.0003	92.86	0.9286	0.0015
	400	0.0002	95.24	0.9524	0.0010
	500	0.0001	97.62	0.9762	0.0005
$[Fe(L)_2(H_2O)_2]$	Blank	0.0060	-	-	0.0300
	100	0.0038	87.50	0.8750	0.0038
	200	0.0040	93.00	0.9300	0.0020
	300	0.0004	93.75	0.9375	0.0019
	400	0.0003	95.83	0.9583	0.0003
	500	0.0001	97.92	0.9792	0.0006
$[Co(L)_2(H_2O)_2]$	Blank	0.0046	-	-	0.0231
	100	0.0010	78.26	0.7826	0.0050
	200	0.0006	86.41	0.8641	0.0031
	300	0.0004	91.85	0.9185	0.0018
	400	0.0003	94.57	0.9457	0.0013
	500	0.0001	97.28	0.9728	0.0006
$[Ni(L)_2(H_2O)]$	Blank	0.0045	-	-	0.0225
	100	0.0020	55.56	0.5556	0.0100
	200	0.0008	83.33	0.8333	0.0038
	300	0.0005	88.89	0.8889	0.0025
	400	0.0004	91.67	0.9167	0.0018
	500	0.0003	94.44	0.9444	0.0013
$Zn(L)_2(2H_2O)$	Blank	0.0059	-	-	0.0295
	100	0.0021	64.41	0.6441	0.0105
	200	0.0008	86.44	0.8644	0.0040
	300	0.0007	88.14	0.8814	0.0035
	400	0.0006	89.83	0.8983	0.0030
	500	0.0004	93.22	0.9322	0.0020

CR: Corrosion rate, IE (%): Percentage inhibition efficiency, Θ: Inhibition efficiency and W: Weight loss

Table 6: Quantum chemical variables

Parameters inhibitors (eV)	LH-chelator	$[Mn(L)_2(H_2O)_2]$	$[Fe(L)_2(H_2O)_2]$	$[Co(L)_2(H_2O)_2]$	$[Ni(L)_2(H_2O)]$	$[Cu(L)_2(H_2O)_2]$	$Zn(L)_22H_2O$
E_{HOMO}	-5.27492	-4.904025	-4.719804	-5.169593	-5.19245851	-4.9862032	-5.288793
E_{LUMO}	-2.07323	-2.400311	-2.389971	-2.552694	-2.1603071	-3.29148187	-2.420447
ΔE	3.20169	2.503714	2.329833	2.616899	3.0321514	1.694721	2.867483
Ionization potential	5.27492	4.904025	4.719804	5.169593	5.192458508	4.9862032	5.288793
Electron Affinity	2.07323	2.400311	2.389971	2.552694	2.1603071	3.29148187	2.420447
Electronegativity χ	3.36741	3.652168	3.5548875	3.861144	3.6763828	4.1388425	3.854689
CH pot	-3.36741	-3.652168	-3.554888	-3.861144	-3.6763828	-4.1388425	-3.854689
Hardness η	1.600845	1.251857	1.1649165	1.308450	1.516075704	0.84736067	1.434173
Softness σ	0.624670	0.798813	0.8584306	0.764263	0.659597668	1.180135019	0.697266
Electrophilicity index ω	4.216168	5.327418	5.4240905	5.696983	4.45749195	10.10786661	5.180207
Chemical potential μ	3.716718	2.159003	4.123912	7.930256	4.813942	6.337552	6.745878

from gravimetric assessment at different doses of the inhibitor(s) at constant temperature and different times. The research demonstrated that as concentrations increased, CR reduced. The drop is due to the inhibitor concentration's inhibitive impact. It was also discovered that as inhibitor concentration rose, IE increased, yielding values of 94.34, 97.62, 97.92, 97.28, 94.44 and 93.22% for LH, Mn(II), Fe(II), Co(II), Ni(II) and Zn(II), respectively. This might be attributed to LH adsorption on the ms surface by bonding free

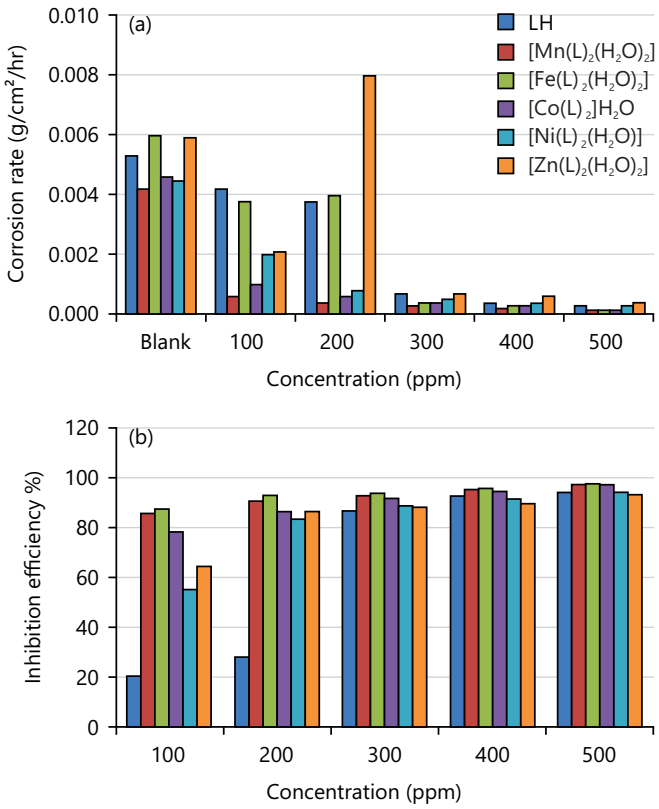

Fig. 1(a-b): Variation of (a) CR and (b) IE against the concentration of LH and its chelates at 303K

electron pairs of N- and O-atoms, as well as electrons of the cyclic rings combining with the imine moiety. The chelates were arranged as follows: Fe(II)>Mn(II)>Co(II)>Ni(II)>LH>Zn (II). This denoted that Fe(II) chelate had the greatest IE (97.92%), while Zn(II) chelate had the lowest (93.22%). The discrepancy in inhibitory performance was most likely due to differences in the chelates' stability and solubility in acid solution[18,50].

Quantum (DFT) studies

Global reactivity: The quantum chemical calculations and DFT methods adopted were as reported in literature[19]. Figure 2 showed the optimized chemical structure of LH and its complexes. Figure 3 depicted the optimized HOMO and LUMO orbital structures for the compounds. As revealed in Table 6, the complexes studied, exhibited greater *E*HOMO data but lesser *E*LUMO data. Zn(II) complex had the highest *E*HOMO value (-5.288793 eV) whereas, Fe(II) complex had the least *E*HOMO value of -4.719804 eV. From the data, the N and O atoms harbored the HOMO levels, making them the preferred electrophilic estimation spots. The latter justifies the adsorption of the chelates on the exterior of the metal, proving their corrosion inhibition potential[21,51]. The *E*HOMO depicts the strength of a molecule in giving out electron[52]. Enhanced *E*HOMO value corroborates *E*LUMO justifying the molecule as an electron donor. The latter depicts the forte of a molecule to accept electron[52], whereas small *E*LUMO values signal that the molecule possesses better electron acceptor potential. The LH ligand had the lowest *E*LUMO with a value of -2.07323 eV, in agreement with experimental data.

The low value of *E* indicates a greater propensity of the inhibitor to be adsorbed on the steel exterior[21,53]. As verified in Table 6, all the complexes displayed a low energy gap (*E*LUMO- *E*HOMO) indicating high reactivity. These Δ*E* values (3.20169, 2.503714, 2.329833, 2.616899, 3.0321514, 1.694721 and 2.867483 eV) designate a transfer of an electron from HOMO to LUMO. This denotes that the complexes have excellent adsorption strength and can increase chemical reactions because they all have low energy gap values, with

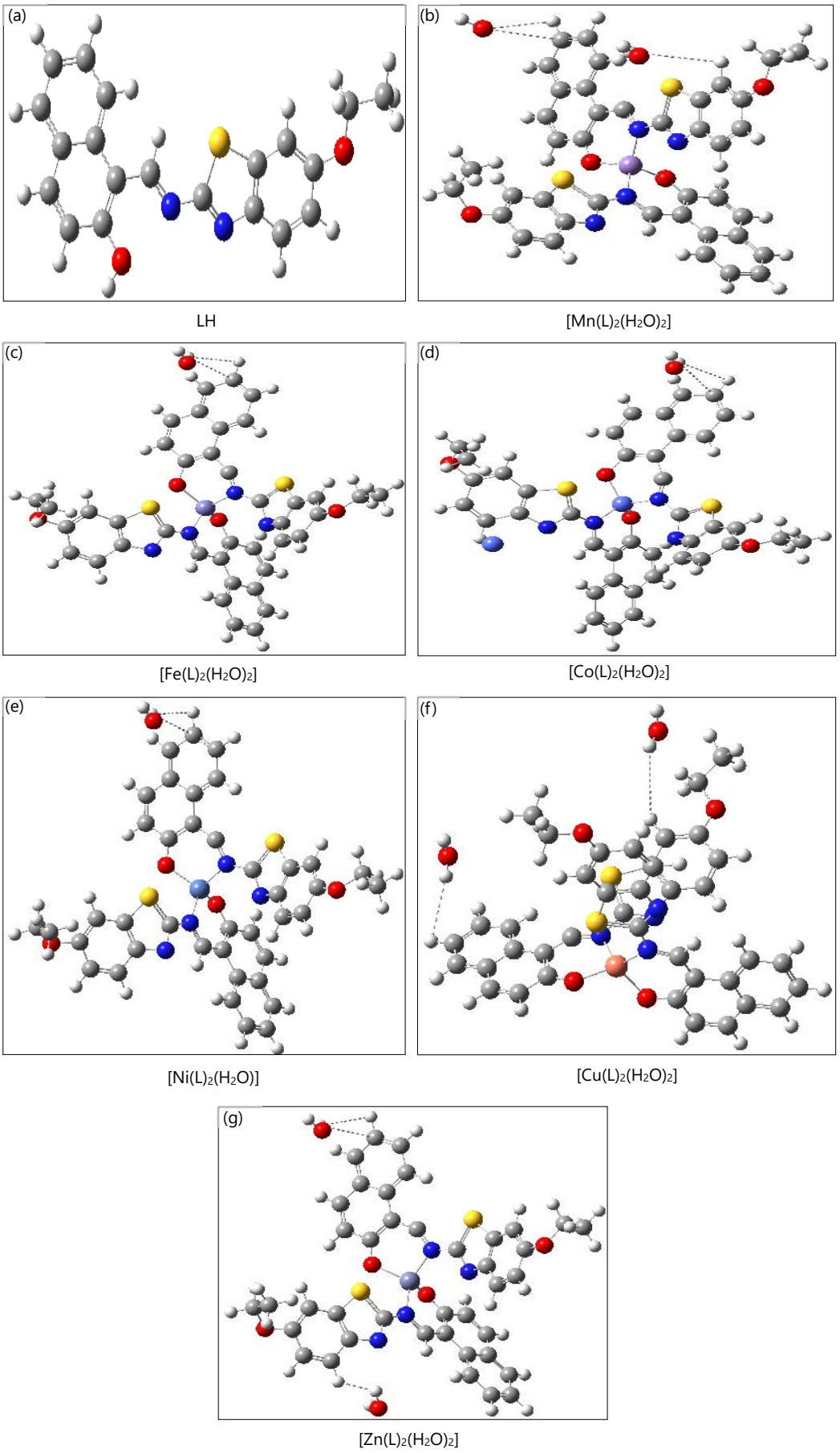

Fig. 2(a-g): Optimized structures for LH and its complexes calculated by B3LYP/6-31G (d, p)

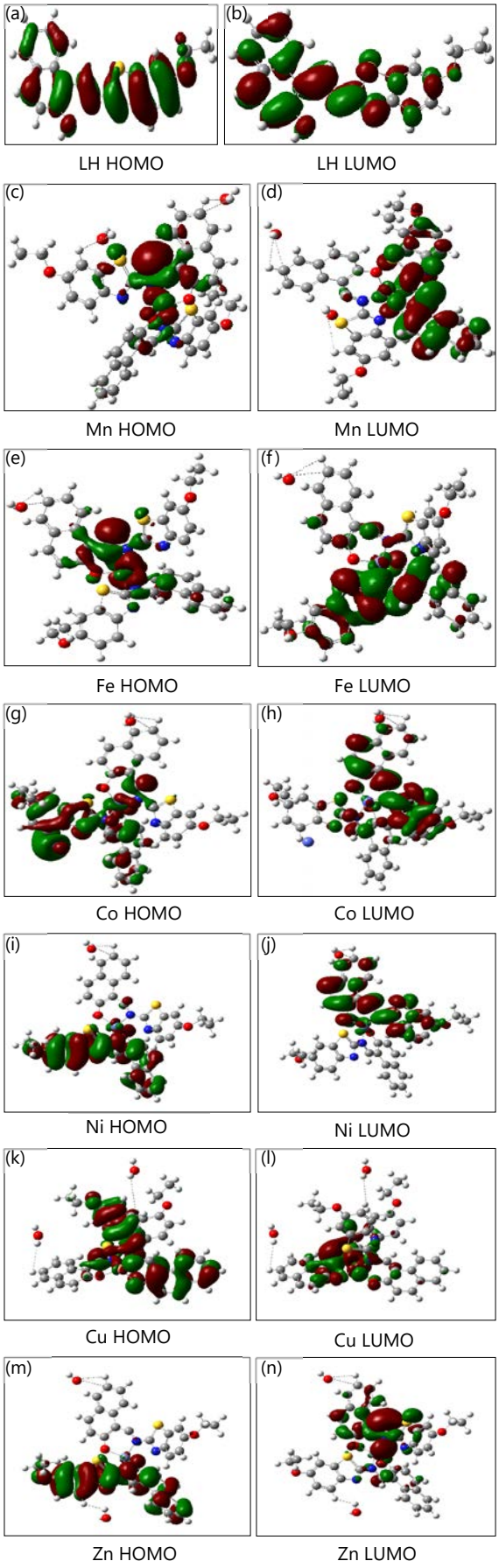

Fig. 3(a-n): HOMO and LUMO diagrams of the chelator and its chelates by B3LYP/6-31G (d, p)

LH having the lowest tendency to accept an electron, indicating a lower tendency for electrons to move to the excited state when compared to its chelates. Because of its lower energy gap, the $[Cu(L)_2(H_2O)_2]$ complex showed a stronger inclination to donate electrons than others (1.694721 eV).

The high χ values depict the potential of inhibitors to receive electrons, forming a strong bond with the metal atom[53], on the other hand, less χ data proves the capability of inhibitor molecules to give out electrons. Many inhibitors display an averagely less χ data suggestive of their strength to give out electrons. The acquired data (Table 6) depicted that the χ of all the compounds were very low indicating that they're all electron donors with $[Cu(L)_2(H_2O)_2]$ complex having the highest value of 4.1388425 eV and LH having the least value of 3.36741 eV[19,54]. Often, compounds are evaluated for firmness plus susceptibility from their *η* or *σ* values. A soft molecule has a small energy gap while a hard molecule has a large energy gap[19]. In this current work, the compounds displayed low energy gaps, hence are soft molecules. They all show strong strength to inhibit electron transfer to the studied steel, giving rise to a strong anticorrosion potential.

To appraise the exclusion value of a compound, dipole moment (DM) is adopted[55]. An increase in DM produces corresponding a rise in the efficiency of the CI[17]. Looking through Table 6, the calculated DM revealed that all studied complexes except $[Mn(L)_2(H_2O)_2]$ (with low DM), possess the tendency to interact with high DM species such as biological systems due to high DM character[31]. The *A* disclosures entire energy needed for a chelator to become an electron acceptor whereas the I depicts the strength of a chelator to become an electron donor[49,51]. The result obtained for I and A for the compounds studied depicts high figures of I and low figures for A corroborating the strength of the compounds both to give and receive electrons. The ω factor estimates chemical reactivity as it affords data on both η and μ of a compound. Higher data of ω were taken to depict a better electrophile while lesser ω data denote nucleophilic strength[51,56,57]. The low electrophilic values of = 4.216168eV (LH), =5.327418 eV ($[Mn(L)_2(H_2O)_2]$), = 5.4240905 eV ($[Fe(L)_2(H_2O)_2]$), = 5.696983 eV ($[Co(L)_2(H_2O)_2]$, = 4.45749195 eV $[Ni(L)_2]$. H_2O, = 10.10786661 eV $[Cu(L)_2(H_2O)_2]$ and = 5.180207 eV $Zn(L)_2(H_2O)_2]$ compounds show they were good nucleophiles which indicate higher chemical reactivity.

CONCLUSION

An imine chelator obtained from the condensation of 2-HNA and 2-AEBT as well as its bivalent chelates has been synthesized and characterized. Additionally, they were examined for biological and CI potentials. A 6-coordinate assemblage was assigned to the bivalent chelates on the basis of UV-vis and ueff data except for Ni(II) chelate which adopted tetrahedral geometry. The low conductance data supported the fact that the chelates were nonelectrolytes. The imine chelator plus its chelates had myriad shades distinctive from their precursors. The FTIR spectrum of the chelator presented a band at 1622 cm^{-1} that shifted to 1616-6220 cm^{-1} in the chelates and was assigned to -C=N- moiety. This present study showed that $[Zn(L)_2(H_2O)_2]$ had the highest antibacterial actions against *Streptococcus* sp. The highest antifungal action was displayed against *A. niger* by $[Mn(L)_2(H_2O)_2]$ chelate (26.5 mm). The effect of imine chelator on acid corrosion of ms could be evident from the result that the chelator showed considerable CI behavior in opposition to corrosion of ms in a 1M HCl solution. The absorption of the composite compounds on the metal surface which was proven by the Density Functional Theory calculations showed that the chelator and its chelates are potential corrosion inhibitors for steel protection.

SIGNIFICANCE STATEMENT

The present study was aimed at establishing the inhibitive potentials of an imine chelator acquired from 2-hydroxyl-1-naphthaldehyde and 2-amino-6-ethoxybenzothiazole and its chelates. The compounds were obtained through reflux-condensation reactions. The chelator was bidentate, while the chelates assumed a 6-coordinate octahedral assemblage. The corrosion-inhibitive data showed that the chelator displayed

considerable corrosion inhibition potentials against the corrosion of mild steel in an HCl solution. Our synthesized $[Zn(L)_2(H_2O)_2]$ chelate had the highest antibacterial actions against *Streptococcus* sp. while the highest antifungal action was displayed against *A. niger* by $[Mn(L)_2(H_2O)_2]$ chelate (26.5mm). Researchers can frontier the data of this research to generate excellent antimicrobial and anti-corrosion agents to solve related problems.

REFERENCES

1. Abu-Dief, A.M. and I.M.A. Mohamed, 2015. A review on versatile applications of transition metal complexes incorporating Schiff bases. Beni-Suef Univ. J. Basic Appl. Sci., 4: 119-133.
2. Mumtaz, A., T. Mahmud, M.R. Elsegood and G.W. Weaver, 2016. Synthesis and characterization of new Schiff base transition metal complexes derived from drug together with biological potential study. J. Nucl. Med. Radiat. Ther., Vol. 7. 10.4172/2155-9619.1000310.
3. Kajal, A., S. Bala, S. Kamboj, N. Sharma and V. Saini, 2013. Schiff bases: A versatile pharmacophore. J. Catal. 10.1155/2013/893512.
4. Mesbah, M., T. Douadi, F. Sahli, S. Issaadi, S. Boukazoula and S. Chafaa, 2018. Synthesis, characterization, spectroscopic studies and antimicrobial activity of three new Schiff bases derived from Heterocyclic moiety. J. Mol. Struct., 1151: 41-48.
5. Sadi, A.H., M.I. Idris and S.S. Bashir, 2017. Synthesis, characterization and antimicrobial studies of Ru(II) complexes with Schiff base co-ligand derived from 5,6-diamino-1,10-phenanthroline and benzene-1,4-dicarbaldehyde. Bayero J. Pure Appl. Sci., 10: 468-476.
6. Soroceanu, A. and A. Bargan, 2022. Advanced and biomedical applications of schiff-base ligands and their metal complexes: A review. Crystals, Vol. 12. 10.3390/cryst12101436.
7. Chioma, F., 2021. Solvo-thermal assisted-synthesis; experimental and theoretical characterization; and biological evaluations of azo-chelator-ligand chelates of Fe(II) and Zn(II) ions. Asian J. Appl. Chem. Res., 10: 40-56.
8. Huang, Z., G. Yang, Z. Lin and J. Huang, 2001. 2-[N^1-2-pyrimidyl-aminobenzenesulfonamido] ethyl 4-bis(2-chloroethyl) aminophenyl butyrate: A potent antitumor agent. Bioorg. Med. Chem. Lett., 11: 1099-1103.
9. Jones, J.S. and F.P. Gabbaï, 2016. Coordination- and redox-noninnocent behavior of ambiphilic ligands containing antimony. Acc. Chem. Res., 49: 857-867.
10. Mohanty, P., S. Behera, R. Behura, L. Shubhadarshinee, P. Mohapatra, A.K. Barick and B.R. Jali, 2022. Antibacterial activity of Thiazole and its derivatives: A review. Biointerface Res. Appl. Chem., 12: 2171-2195.
11. Thakar, A.S., K.K. Singh, K.T. Joshi, A.M. Pancholi and K.S. Pandya, 2010. Synthesis, characterization and antibacterial activity of schiff bases and their metal complexes derived from 4-acyl-1-phenyl-3-methyl-2-pyrazolin-5-ones and 2-amino-4(4'-methylphenyl)-thiazole. J. Chem., 7: 1396-1406.
12. Petrou, A., M. Fesatidou and A. Geronikaki, 2021. Thiazole ring-a biologically active scaffold. Molecules, Vol. 26. 10.3390/molecules26113166.
13. Minickaitė, R., B. Grybaitė, R. Vaickelionienė, P. Kavaliauskas and V. Petraitis *et al*., 2022. Synthesis of novel aminothiazole derivatives as promising antiviral, antioxidant and antibacterial candidates. Int. J. Mol. Sci., Vol. 23. 10.3390/ijms23147688.
14. Elsadek, M.F., B.M. Ahmed and M.F. Farahat, 2021. An overview on synthetic 2-aminothiazole-based compounds associated with four biological activities. Molecules, Vol. 26. 10.3390/molecules26051449.
15. Fayomi, O.S.I., D. Olusanyan, F.T. Ademuyiwa and G. Olarewaju, 2021. Progresses on mild steel protection toward surface service performance in structural industrial: An overview. IOP Conf. Ser.: Mater. Sci. Eng., Vol. 1036. 10.1088/1757-899X/1036/1/012079.
16. Shetty, P., 2020. Schiff bases: An overview of their corrosion inhibition activity in acid media against mild steel. Chem. Eng. Commun., 207: 985-1029.

17. Singh, A., K.R. Ansari, M.A. Quraishi and S. Kaya, 2020. Theoretically and experimentally exploring the corrosion inhibition of N80 steel by pyrazol derivatives in simulated acidizing environment. J. Mol. Struct., Vol. 1206. 10.1016/j.molstruc.2020.127685.
18. Festus, C. and C.T. Wodi, 2021. Corrosion inhibition; and antimicrobial studies of bivalent complexes of 1-(((5-ethoxybenzo[d]thiazol-2-yl) Imino) methyl) naphthalene-2-ol chelator: Design, synthesis, and experimental characterizations. Direct Res. J. Chem. Mater. Sci., 8: 31-43.
19. Chioma, F. and W.C. Theresa, 2022. Novel M^{2+} complexes of 2-(thiazol-2-ylamino)-2, 3-dihydronaphthalene-1,4-dione schiff base: Design, preparation, characterizations and corrosion inhibition studies. J. Appl. Sci., 22: 152-165.
20. Chioma, F. and C.D. Don-Lawson, 2018. Synthesis, spectral, magnetic and *in-vitro* biological studies of organic ligands and their corresponding heteroleptic divalent d-metal complexes. Pharm. Chem. J., 5: 118-129.
21. Festus, C., O.A. Ekpete and C.D. Don-Lawson, 2020. Novel metal^{2+} complexes of n-(1,4-dihydro-1,4-oxonaphthalen-3-yl) pyrazine-2-carboxamide: Synthesis, structural characterization, magnetic properties and antimicrobial activities. Curr. Res. Chem., 12: 1-10.
22. Neelofar, N., N. Ali, A. Khan, S. Amir, N. A. Khan and M. Bilal, 2017. Synthesis of Schiff bases derived from 2-hydroxy-1-naphth-aldehyde and their tin(II) complexes for antimicribial and antioxidant activities. Bull. Chem. Soc. Ethiop., 31: 445-456.
23. Wodi, T.C., C. Festus and E. Nlemonwu, 2022. Anti-corrosive potentials of naphtho-quinone/naphtha-aldehyde schiff bases for mild steel in HCL medium: Synthesis, characterization and DFT studies. J. Chem. Soc. Niger., 47: 1075-1098.
24. Gomathi, V. and R. Selvameena, 2013. Synthesis, spectroscopic, electrochemical and biological studies of novel schiff base complexes derived from 4-(3-ethoxy-2-hydroxybenzylideneamino)-N-(pyridin-2-yl)benzenesulfonamide. Main Group Chem., 12: 275-284.
25. Iroha, N.B. and N.A. Madueke, 2018. Effect of *Triumfetta rhomboidea* leaves extract on the corrosion resistance of carbon steel in acidic environment. Chem. Sci. Int. J., Vol. 25. 10.9734/CSJI/2018/45807.
26. Abdul Ghani, A., H. Bahron, M.K. Harun and K. Kassim, 2012. Corrosion inhibition study of a heterocyclic Schiff base derived from Isatin. Adv. Mater. Res., 554-556: 425-429.
27. Chioma, F., A.C. Ekennia, A.A. Osowole, S.N. Okafor, C.U. Ibeji, D.C. Onwudiwe and O.T. Ujam, 2018. Synthesis, characterization, *in-vitro* antimicrobial properties, molecular docking and DFT studies of 3-{(*E*)-[(4,6-dimethylpyrimidin-2-yl)imino]methyl} naphthalen-2-ol and heteroleptic Mn(II), Co(II), Ni(II) and Zn(II) complexes. Open Chem., 16: 184-200.
28. Shah, S.S., D. Shah, I. Khan, S. Ahmad, U. Ali and Atiq ur Rahman, 2020. Synthesis and antioxidant activities of Schiff bases and their complexes: An updated review. Biointerface Res. Appl. Chem., 10: 6936-6963.
29. Kpee, F., C.V. Ukachukwu and C. Festus, 2018. Synthesis, characterization and extractive potentials of aminopyrimidine Schiff base ligands on divalent metal ions. Niger. Res. J. Chem. Sci., 4: 193-203.
30. Chioma, F., O.W. Nnenna and O. Moses, 2020. Preparation, spectral characterization and corrosion inhibition studies of (*E*)-*N*-{(thiophene-2-yl)methylene}pyrazine-2-carboxamide Schiff base ligand. Prot. Metals Phys. Chem. Surf., 56: 651-662.
31. Chioma, F., C.I. Ezugwu and O. Okpareke, 2023. Synthesis, characterization, DFT and biological studies of Fe(II), Cu(II), and Zn(II) complexes of keto-imine chelators. Inorg. Chim. Acta, Vol. 545. 10.1016/j.ica.2022.121255.
32. Alturiqi, A.S., A.N.M.A. Alaghaz, R.A. Ammar and M.E. Zayed, 2018. Synthesis, spectral characterization, and thermal and cytotoxicity studies of Cr(III), Ru(III), Mn(II), Co(II), Ni(II), Cu(II), and Zn(II) complexes of Schiff base derived from 5-hydroxymethylfuran-2-carbaldehyde. J. Chem., Vol. 2018. 10.1155/2018/5816906.
33. Abbas, S.F., J.H. Tomma and E.T. Ali, 2021. Synthesis and characterization of new Schiff bases and their 1,3-oxazepines derived from phthalic anhydride. Syst. Rev. Pharm., 12: 260-265.

34. Yu, F., Z. Wang, S. Zhang, H. Ye and K. Kong *et al*., 2018. Molecular engineering of donor-acceptor conjugated polymer/g-C_3N_4 heterostructures for significantly enhanced hydrogen evolution under visible-light irradiation. Adv. Funct. Mater., Vol. 28. 10.1002/adfm.201804512.
35. Aliyu, H.N. and U. Sani, 2012. Synthesis, characterization and biological activity of manganese(II), iron(II), cobalt(II), nickel(II) and copper(II) Schiff base complexes against multidrug resistant bacterial and fungal pathogens. Int. Res. J. Pharm. Pharmacol., 2: 40-44.
36. Turan, N. and K. Buldurun, 2018. Synthesis, characterization and antioxidant activity of Schiff base and its metal complexes with Fe(II), Mn(II), Zn(II), and Ru(II) ions: Catalytic activity of ruthenium(II) complex. Eur. J. Chem., 9: 22-29.
37. Ajlouni, A.M., Z.A. Taha, K.A. Al-Hassan and A.M. Abu Anzeh, 2012. Synthesis, characterization, luminescence properties and antioxidant activity of Ln(III) complexes with a new aryl amide bridging ligand. J. Lumin., 132: 1357-1363.
38. Festus, C., A.C. Ekennia, A.A. Osowole, L.O. Olasunkanmi, D.C. Onwudiwe and O.T. Ujam, 2018. Synthesis, experimental and theoretical characterization and antimicrobial studies of some Fe(II), Co(II) and Ni(II) complexes of 2-(4,6-dihydroxypyrimidin-2-ylamino)naphthalene-1,4-dione. Res. Chem. Intermed., 44: 5857-5877.
39. Cotton, F.A., G. Wlkinson, C.A. Murillo and M. Bochmann, 1999. Advanced Inorganic Chemistry. 6th Edn., John Wiley & Sons, United States, ISBN: 978-0-471-19957-1, Pages: 1376.
40. Chioma, F., C.U. Ibeji and O. Okpareke, 2020. Novel 3d divalent metallic complexes of 3-[(2-hydroxy-5-methyl-phenylimino)-methyl]-napthalen-2-ol: Synthesis, spectral characterization, antimicrobial and computational studies. J. Mol. Struct., Vol. 1210. 10.1016/j.molstruc.2020.128017.
41. Munde, A.S., V.A. Shelke, S.M. Jadhav, A.S. Kirdant, S.R. Vaidya, S.G. Shankarwar and T.K. Chondhekar, 2012. Synthesis, characterization and antimicrobial activities of some transition metal complexes of biologically active asymmetrical tetradentate ligands. Adv. Appl. Sci. Res., 3: 175-182.
42. Tisato, F., F. Refosco, G. Bandoli, C. Bolzati and A. Moresco, 1994. Synthesis and characterization of neutral technetium(III) complexes with mixed S,P-bidentate phosphine-thiolate ligands. Crystal structure of $[Tc(SCH_2CH_2PPh_2)_2(SCH_2CH_2PPh_2O)]$. J. Chem. Soc., Dalton Trans., 23: 1453-1461.
43. Mapari, A.K. and K.V. Mangaonkar, 2011. Synthesis, characterization and antimicrobial activity of mixed schiff base ligand complexes of transition metal(II) ions. Int. J. ChemTech Res., 3: 477-482.
44. Lather, P., A.K. Mohanty, P. Jha and A.K. Garsa, 2016. Contribution of cell surface hydrophobicity in the resistance of *Staphylococcus aureus* against antimicrobial agents. Biochem. Res. Int., Vol. 2016. 10.1155/2016/1091290.
45. Gonelimali, F.D., J. Lin, W. Miao, J. Xuan, F. Charles, M. Chen and S.R. Hatab, 2018. Antimicrobial properties and mechanism of action of some plant extracts against food pathogens and spoilage microorganisms. Front. Microbiol., Vol. 9. 10.3389/fmicb.2018.01639.
46. Chaturvedi, D. and M. Kamboj, 2016. Role of Schiff base in drug discovery research. Chem. Sci. J., Vol. 7. 10.4172/2150-3494.1000E114.
47. El-Sherif, A.A., M.M. Shoukry and M.M. Abd-Elgawad, 2012. Synthesis, characterization, biological activity and equilibrium studies of metal(II) ion complexes with tridentate hydrazone ligand derived from hydralazine. Spectrochim. Acta Part A: Mol. Biomol. Spectrosc., 98: 307-321.
48. Jacob, K.S. and G. Parameswaran, 2010. Corrosion inhibition of mild steel in hydrochloric acid solution by Schiff base furoin thiosemicarbazone. Corros. Sci., 52: 224-228.
49. Odozi, N.W., F. Chioma and M.A. Dagoli, 2020. Synthesis, adsorption and inhibition behaviour of 2-[(thiophen-2-ylmethylidene) amino] pyridine-3-ol on mild steel corrosion in aggressive acidic media. Niger. Res. J. Chem. Sci., 8: 291-307.
50. Yadav, M., 2012. Synthesis, characterization, and biological activity of some transition metal complexes of N-benzoyl-N -2-thiophenethiocarbohydrazide. Int. J. Inorg. Chem., Vol. 2012. 10.1155/2012/269497.
51. Gouda, M., M.M. Khalaf, K. Shalabi, M.A. Al-Omair and H.M. Abd El-Lateef, 2022. Synthesis and characterization of Zn-organic frameworks containing chitosan as a low-cost inhibitor for sulfuric-acid-induced steel corrosion: Practical and computational exploration. Polymers, Vol. 14. 10.3390/polym14020228.

52. Popova, A., M. Christov and T. Deligeorgiev, 2003. Influence of the molecular structure on the inhibitor properties of benzimidazole derivatives on mild steel corrosion in 1 M hydrochloric acid. Corros. J. Sci. Eng., 59: 756-764.
53. Abd El-Lateef, H.M., K. Shalabi and A.H. Tantawy, 2020. Corrosion inhibition of carbon steel in hydrochloric acid solution using newly synthesized urea-based cationic fluorosurfactants: Experimental and computational investigations. New J. Chem., 44: 17791-17814.
54. Upadhyay, A., A.K. Purohit, G. Mahakur, S. Dash and P.K. Kar, 2021. Verification of corrosion inhibition of mild steel by some 4-aminoantipyrine-based Schiff bases-impact of adsorbate substituent and cross-conjugation. J. Mol. Liq., Vol. 333. 10.1016/j.molliq.2021.115960.
55. Oyebamiji, A.K. and B.B. Adeleke, 2018. Quantum chemical studies on inhibition activities of 2,3-dihydroxypropyl-sulfanyl derivative on carbon steel in acidic media. Int. J. Corros. Scale Inhib., 7: 498-508.
56. Bououden, W. and Y. Benguerba, 2020. Designing, cytotoxic evaluation, molecular docking and *in silico* pharmacokinetic prediction of new hydrocortisone derivatives as anti-asthmatics drugs. J. Drug Delivery Ther., 10: 8-16.
57. Diki, N.Y.S., N.H. Coulibaly, O. Kambiré and A. Trokourey, 2021. Experimental and theoretical investigations on copper corrosion inhibition by cefixime drug in 1M HNO_3 solution. J. Mater. Sci. Chem. Eng., 9: 11-28.